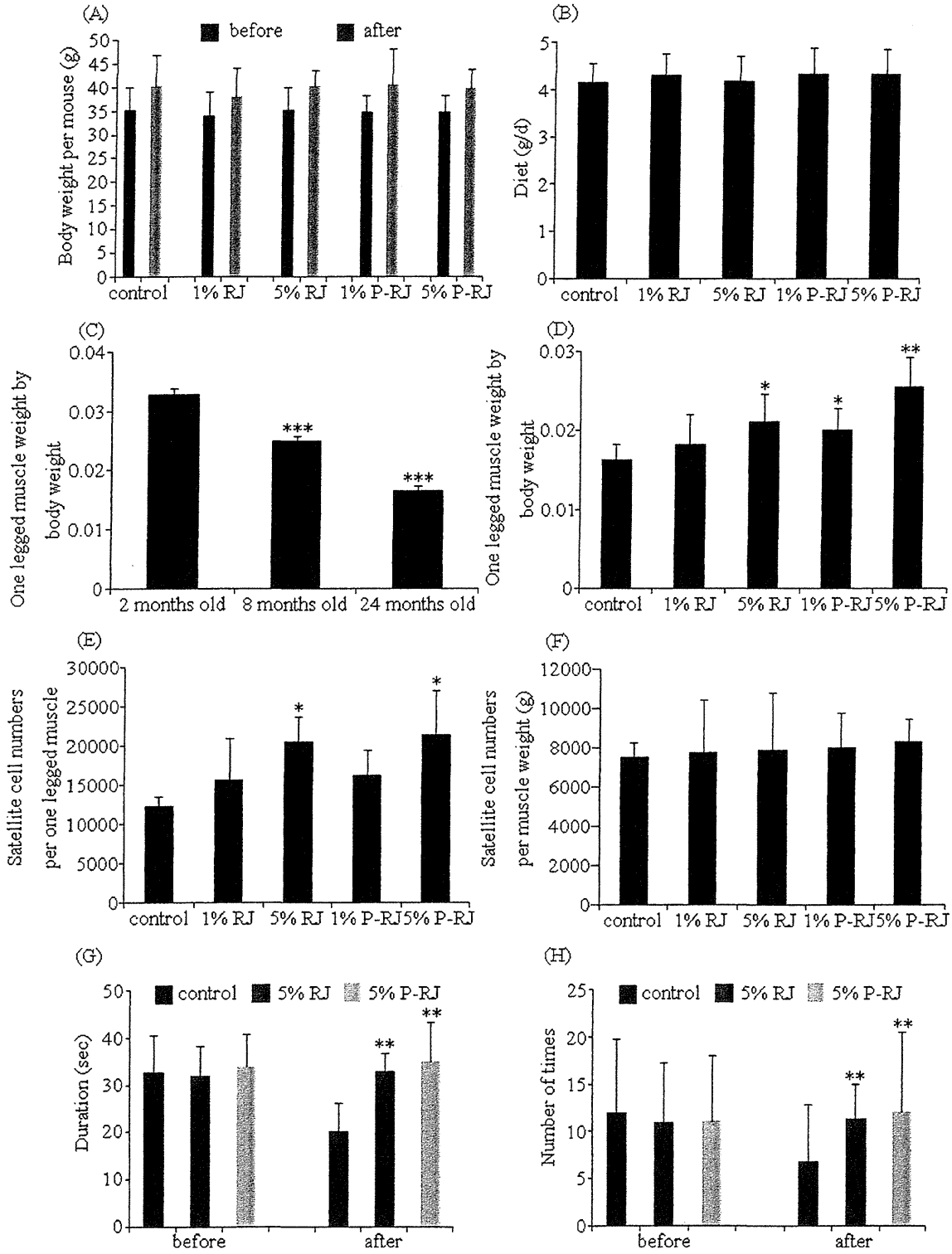

Figure 3. Effects of RJ/pRJ treatment on aged mice in vivo. Twenty-one-month-old mice were treated with a diet mixed with 1% weight RJ (1% RJ), diet with 5% weight RJ (5% RJ), diet with 1% weight pRJ (1% pRJ), or diet with 5% pRJ (5% pRJ) for following 3 months. (**A**) Control, RJ, or pRJ treatment did not show changed body weight. (**B**) RJ or pRJ did not change the amount of the daily diet intake. (**C**) The progressive loss of muscle weight with aging. (**D**) RJ- and pRJ-treated groups had greater hind-limb muscle weights per body weight than did controls. (**E**) RJ- and pRJ-treated groups had greater numbers of satellite cells in the hind-limb muscles than did controls. (**F**) RJ or pRJ treatment did not change the numbers of satellite cells per muscle weight (g). (**G**) Five% RJ- and pRJ-treated mice hung for longer durations than did controls. (**H**) Five% RJ- and pRJ-treated mice hung more times than did controls. Columns are mean ± *SD*, $n \geq 5$ in each group. $^{*}p < .05$, $^{**}p < .01$, and $^{***}p \leq .0001$ compared with control.

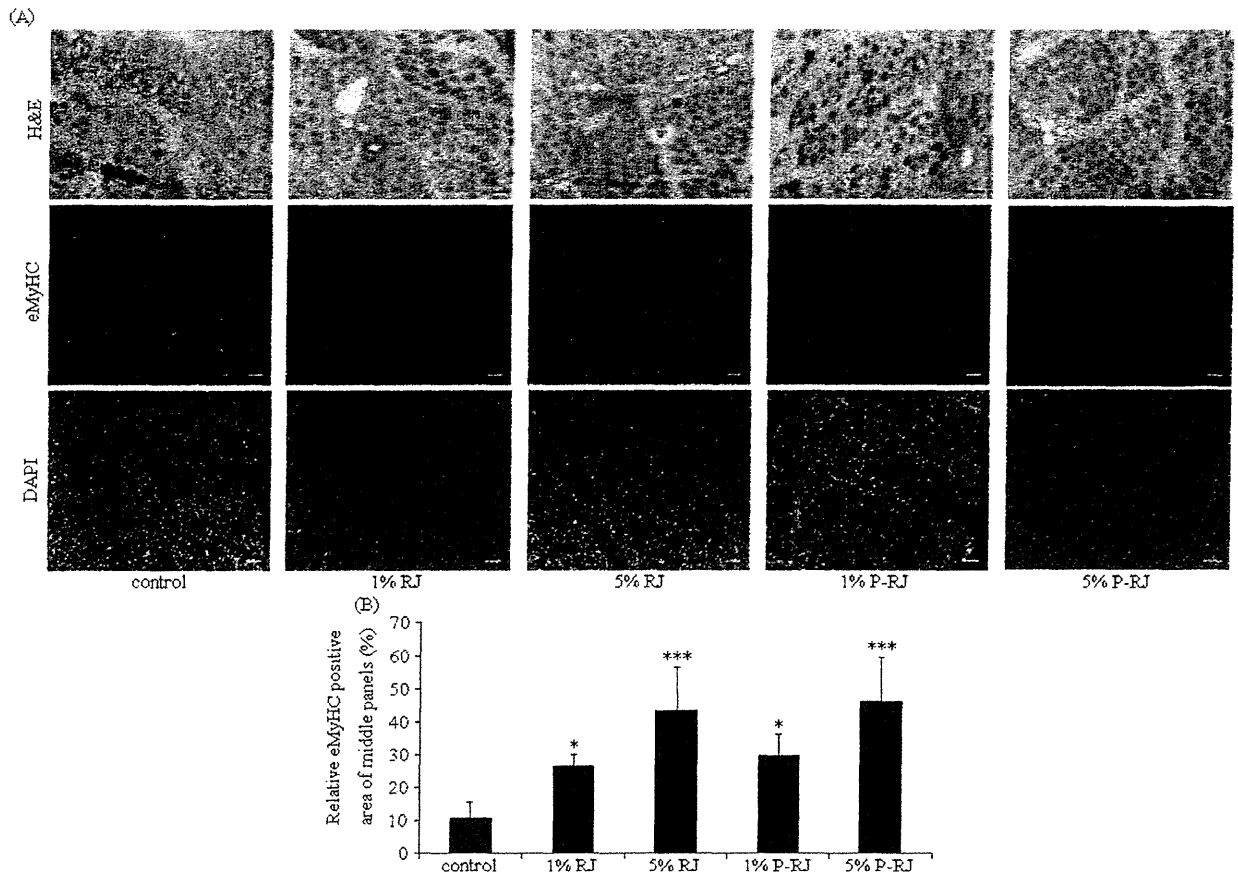

Figure 4. RJ/pRJ treatment accelerated the regeneration of the injured skeletal muscles in aged mice. After 3 months of RJ/pRJ treatment, we injected cardiotoxin into the tibialis anterior muscles of the aged mice to injure the muscles and isolated them 5 days later. (**A**) Hematoxylin and eosin staining (top panels) and immunohistochemical staining for eMyHC (middle panels) or DAPI (bottom panels) of the injured tibialis anterior muscles. Upper lines, scale bar, 50 μm; middle and lower lines, scale bar, 100 μm. (**B**) The graph shows the data calculated from quantification of the percentage of eMyHc-immunoreactive area per field for each group (10 randomly selected fields at ×200 magnification per sample were quantified). Columns are mean ± *SD*, $n \geq 3$ in each group. $^{*}p < .05$, and $^{***}p < .0001$ compared with controls.

We chose IL-1α, IL-1β, IL-6, and tumor necrosis factor-α as proinflammatory mediators, as previously shown (31,32), and measured their levels in serum. The levels of these mediators were not significantly different between RJ-/pRJ-treated groups and controls, but the serum IL-1α concentration tended to be lower in the RJ/pRJ groups than in the controls (Figure 5A). Because IGF-1 plays a central role in stimulating satellite cells, we measured the serum levels of IGF-1. The serum levels of IGF-1 were greater in the 5% RJ- and pRJ-treated groups than in the controls (Figure 5B).

Discussion

In this study, using aged mice, we showed that RJ/pRJ treatment increased the number of satellite cells, the skeletal muscle weight, grip strength, regenerating capacity of injured skeletal muscles, and the serum IGF-1 levels compared with controls in vivo. In vitro, compared with controls, pRJ treatment increased the cell proliferation rate, promoted differentiation, and activated the Akt-signaling pathway in the satellite cells of the aged mice.

RJ/pRJ treatment increased the number of satellite cells of the aged mice, promoted their differentiation compared with controls, which could be the mechanisms by which the skeletal muscle weight and grip strength were increased, and accelerated the regeneration of injured skeletal muscles in aged mice compared with controls. Because these effects antagonized the loss of muscle mass and strength, the results suggested that RJ/pRJ treatment might improve sarcopenia in aged mice. The RJ-/pRJ-treated groups hung for longer durations than did the controls, but when we compared between before and after the treatment period within the same groups, the hanging duration did not change in the RJ-/pRJ-treated groups, whereas the hanging duration decreased after the same period in controls, suggesting that RJ/pRJ treatment might not improve but rather attenuated the progression of the decrease in grip strength. Therefore, the effects of RJ/pRJ on skeletal muscles might be

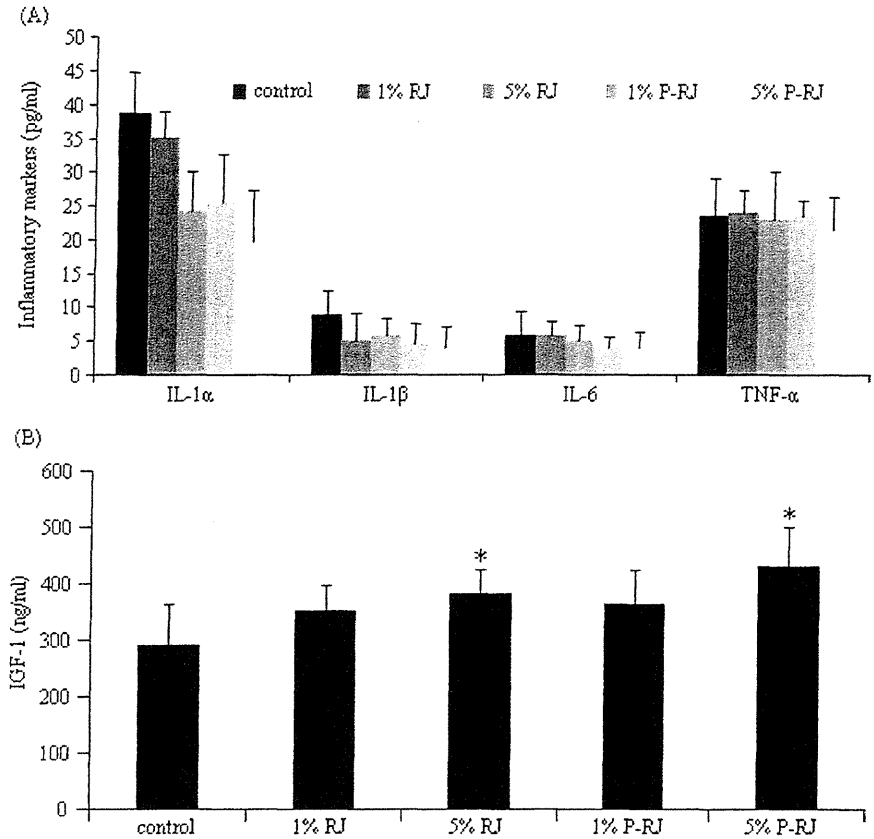

Figure 5. RJ/pRJ treatment increased the serum IGF-1 levels but did not affect the serum proinflammatory mediator levels. ELISA determined serum levels of proinflammatory mediators and IGF-1 in aged mice treated with RJ/pRJ for 3 months. (**A**) RJ/pRJ treatment did not change the serum levels of the proinflammatory mediators. (**B**) Five% RJ and 5% pRJ treatment significantly increased the serum IGF-1 levels. Columns are mean ± *SD*, $n = 5$ in each group. *$p < .05$ compared with controls.

attenuating the atrophy rather than improving the muscle mass and strength in aged mice.

pRJ increased the number of satellite cells of the aged mice in vivo and in vitro, whereas RJ increased the number of the satellite cells in vivo but not in vitro. The presence of protease treatment in pRJ and its absence in RJ might explain this discrepancy. Protease is present in vivo, which indicates that all the RJ is treated with protease after their intake in vivo, whereas protease is not present in vitro.

Because IGF-1 has favorable effects on satellite cells, the skeletal muscles, and sarcopenia, the increased serum levels of IGF-1 after RJ/pRJ treatment might be one of the mechanisms of the effects of RJ/pRJ treatment. However, the increases in the levels of IGF-1 after RJ/pRJ treatment were moderate. Therefore, RJ/pRJ treatment may have other mechanisms besides increasing IGF-1. Previous studies indicated that nutrition plays a central role in the regulation of the IGF-1 levels (33). The serum IGF-1 levels decline in an age-dependent manner and are a reliable index of protein-energy malnutrition in elderly patients (34–36). Increased serum levels of IGF-1 after RJ/pRJ treatment may suggest that RJ/pRJ treatment improved the malnutrition in the aged animals. Many nutritional components in RJ/pRJ such as vitamins, minerals (Table 1), and amino acids might have contributed to preventing sarcopenia. Because this is a single study, we could not evaluate the contribution of each component to the prevention of sarcopenia. However, the results suggested that whole RJ/pRJ improved sarcopenia in aged mice.

Akt-signaling pathway plays a central role in muscle protein synthesis and in inhibiting muscle proteolysis. Akt activation prevents muscle atrophy including sarcopenia (37). Moreover, the activation of Akt in myoblasts increased their cell proliferation rate and rescued them from cell death (22). In vitro, pRJ activated the Akt-signaling pathway in satellite cells of the aged mice. Because pRJ contains a wide variety of components (9), it is not clear which component(s) activated Akt. However, the activation of Akt, possibly by IGF-1, suggests that one of the mechanisms of the effects of RJ/pRJ was via Akt. Furthermore, because RJ and pRJ are natural products, some natural factors such as seasonal or environmental factors may affect the percentage or quality of ingredients in RJ/pRJ. Further studies are required to identify the mechanisms of action of RJ/pRJ.

Some studies reported that IGF-1 deficiency extended life spans in mammals (38,39). Because we did not assess life

spans in this study, the effect of increased levels of IGF-1 by RJ/pRJ treatment on life span was not clear. However, previous studies reported that RJ/pRJ extended the life span in mice and *Caenorhabditis elegans* (10,11). Further studies are required to evaluate the effects and mechanisms of RJ/pRJ on life span.

Dietary supplementation with 1%–5% RJ/pRJ would be too great in an amount and would not be feasible for humans. Generally, dietary supplementation intake in animals cannot be directly converted into human dietary intake. Thus, we did a pilot study to examine the effect of RJ on muscle strength and physical performance in free-living elderly patients (Identifier: UMIN000004057, Trial Registration: http://www.umin.ac.jp/ctr/index.htm). We found that the intake of RJ (low dose: 1.2 g/day; high dose: 4.8 g/day) for 3 months improved muscle strength and physical performance in the elderly patients. Based on this pilot study, we are performing a randomized, double-blinded, placebo-controlled trial to confirm the effects of RJ on muscle strength and physical performance of the elderly patients (Identifier: UMIN000009648, Trial Registration: http://www.umin.ac.jp/ctr/index.htm).

In conclusion, in vivo, RJ/pRJ treatment increased the muscle weight, grip strength, regenerating capacity of injured muscles, and serum IGF-1 levels compared with controls in aged mice. In vitro, pRJ increased the cell proliferation rate, promoted the cell differentiation, and activated Akt-signaling pathway compared with controls in isolated satellite cells from aged mice. These findings suggest that RJ/pRJ treatment may have a beneficial effect on the prevention of age-related sarcopenia through increasing the systemic IGF-1 levels and activating Akt-signaling pathways in satellite cells.

FUNDING

This research was supported by Yamada Research Grant.

CONFLICT OF INTERESTS

All the authors have no conflicts of interest to disclose.

REFERENCES

1. Nations United. *Department of Economic and Social Affairs Population Division: World Population Ageing 2009*. New York: United Nations; 2009:11.
2. Altun M, Grönholdt-Klein M, Wang L, Ulfhake B. Cellular degradation machineries in age-related loss of muscle mass (Sarcopenia). In: Nagata T, ed. *Senescence*. San Francisco, CA: Academia.edu; 2012:269–286.
3. Hawke TJ, Garry DJ. Myogenic satellite cells: physiology to molecular biology. *J Appl Physiol*. 2001;91:534–551.
4. Clemmons DR. Role of IGF-I in skeletal muscle mass maintenance. *Trends Endocrinol Metab*. 2009;20:349–356.
5. Welle S. Cellular and molecular basis of age-related sarcopenia. *Can J Appl Physiol*. 2002;27:19–41.
6. Sacco A, Doyonnas R, Kraft P, Vitorovic S, Blau HM. Self-renewal and expansion of single transplanted muscle stem cells. *Nature*. 2008;456:502–506.
7. Giovannini S, Marzetti E, Borst SE, Leeuwenburgh C. Modulation of GH/IGF-1 axis: potential strategies to counteract sarcopenia in older adults. *Mech Ageing Dev*. 2008;129:593–601.
8. Viuda-Martos M, Ruiz-Navajas Y, Fernández-López J, Pérez-Alvarez JA. Functional properties of honey, propolis, and royal jelly. *J Food Sci*. 2008;73:R117–R124.
9. Sabatini AG, Marcazzan GL, Caboni MF, Bogdanov S, Almeida-Muradian LBd. Quality and standardisation of Royal Jelly. *J ApiProduct ApiMedical Sci*. 2009;1:1–6.
10. Inoue S, Koya-Miyata S, Ushio S, Iwaki K, Ikeda M, Kurimoto M. Royal Jelly prolongs the life span of C3H/HeJ mice: correlation with reduced DNA damage. *Exp Gerontol*. 2003;38:965–969.
11. Honda Y, Fujita Y, Maruyama H, et al. Lifespan-extending effects of royal jelly and its related substances on the nematode Caenorhabditis elegans. *PLoS One*. 2011;6:e23527.
12. Kamakura M, Mitani N, Fukuda T, Fukushima M. Antifatigue effect of fresh royal jelly in mice. *J Nutr Sci Vitaminol (Tokyo)*. 2001;47:394–401.
13. Matsui T, Yukiyoshi A, Doi S, Sugimoto H, Yamada H, Matsumoto K. Gastrointestinal enzyme production of bioactive peptides from royal jelly protein and their antihypertensive ability in SHR. *J Nutr Biochem*. 2002;13:80–86.
14. Vittek J. Effect of royal jelly on serum lipids in experimental animals and humans with atherosclerosis. *Experientia*. 1995;51:927–935.
15. Liu JR, Yang YC, Shi LS, Peng CC. Antioxidant properties of royal jelly associated with larval age and time of harvest. *J Agric Food Chem*. 2008;56:11447–11452.
16. Kohno K, Okamoto I, Sano O, et al. Royal jelly inhibits the production of proinflammatory cytokines by activated macrophages. *Biosci Biotechnol Biochem*. 2004;68:138–145.
17. Macaluso A, De Vito G. Muscle strength, power and adaptations to resistance training in older people. *Eur J Appl Physiol*. 2004;91:450–472.
18. Strasser EM, Wessner B, Roth E. Cellular regulation of anabolism and catabolism in skeletal muscle during immobilisation, aging and critical illness. *Wien Klin Wochenschr*. 2007;119:337–348.
19. Schaap LA, Pluijm SM, Deeg DJ, Visser M. Inflammatory markers and loss of muscle mass (sarcopenia) and strength. *Am J Med*. 2006;119:526.e9–526.17.
20. Meng SJ, Yu LJ. Oxidative stress, molecular inflammation and sarcopenia. *Int J Mol Sci*. 2010;11:1509–1526.
21. Sriram S, Subramanian S, Sathiakumar D, et al. Modulation of reactive oxygen species in skeletal muscle by myostatin is mediated through NF-κB. *Aging Cell*. 2011;10:931–948.
22. Okazaki T, Ebihara S, Asada M, et al. Macrophage colony-stimulating factor improves cardiac function after ischemic injury by inducing vascular endothelial growth factor production and survival of cardiomyocytes. *Am J Pathol*. 2007;171:1093–1103.
23. Yahiaoui L, Gvozdic D, Danialou G, Mack M, Petrof BJ. CC family chemokines directly regulate myoblast responses to skeletal muscle injury. *J Physiol*. 2008;586:3991–4004.
24. Okazaki T, Ebihara S, Asada M, Yamanda S, Niu K, Arai H. Erythropoietin promotes the growth of tumors lacking its receptor and decreases survival of tumor-bearing mice by enhancing angiogenesis. *Neoplasia*. 2008;10:932–939.
25. Nakajima R, Takao K, Huang SM, et al. Comprehensive behavioral phenotyping of calpastatin-knockout mice. *Mol Brain*. 2008;7:1–15.
26. Uezumi A, Fukada S, Yamamoto N, Takeda S, Tsuchida K. Mesenchymal progenitors distinct from satellite cells contribute to ectopic fat cell formation in skeletal muscle. *Nat Cell Biol*. 2010;12:143–152.
27. Niu K, Asada M, Okazaki T, et al. Adiponectin pathway attenuates malignant mesothelioma cell growth. *Am J Respir Cell Mol Biol*. 2012;46:515–523.
28. Fukada S, Yamaguchi M, Kokubo H, et al. Hesr1 and Hesr3 are essential to generate undifferentiated quiescent satellite cells and to maintain satellite cell numbers. *Development*. 2011;138:4609–4619.
29. Asada M, Ebihara S, Yamanda S, et al. Depletion of serotonin and selective inhibition of 2B receptor suppressed tumor angiogenesis by

inhibiting endothelial nitric oxide synthase and extracellular signal-regulated kinase ½ phosphorylation. *Neoplasia*. 2009;11:408–417.
30. Yamanda S, Ebihara S, Asada M, et al. Role of ephrinB2 in non-productive angiogenesis induced by Delta-like 4 blockade. *Blood*. 2009;113:3631–3639.
31. Okazaki T, Sakon S, Sasazuki T, et al. Phosphorylation of serine 276 is essential for p65 NF-kappaB subunit-dependent cellular responses. *Biochem Biophys Res Commun*. 2003;300:807–812.
32. Okazaki T, Ni A, Baluk P, et al. Capillary defects and exaggerated inflammatory response in the airways of EphA2-deficient mice. *Am J Pathol*. 2009;174:2388–2399.
33. Chevenne D, Porquet D. Growth hormone (GH) and insulin-like growth factor 1 (IGF-1) in nutritional status. *Ann Biol Clin (Paris)*. 1995;53:527–538.
34. Campillo B, Paillaud E, Bories PN, Noel M, Porquet D, Le Parco JC. Serum levels of insulin-like growth factor-1 in the three months following surgery for a hip fracture in elderly: relationship with nutritional status and inflammatory reaction. *Clin Nutr*. 2000;19:349–354.
35. Ponzer S, Tidermark J, Brismar K, Söderqvist A, Cederholm T. Nutritional status, insulin-like growth factor-1 and quality of life in elderly women with hip fractures. *Clin Nutr*. 1999;18:241–246.
36. McWhirter JP, Ryan MF, Pennington CR. An evaluation of insulin-like growth factor-1 as an indicator of nutritional status. *Clin Nutr*. 1995;14:74–80.
37. Kandarian SC, Jackman RW. Intracellular signaling during skeletal muscle atrophy. *Muscle Nerve*. 2006;33:155–165.
38. Carter CS, Ramsey MM, Ingram RL, et al. Models of growth hormone and IGF-1 deficiency: applications to studies of aging processes and life-span determination. *J Gerontol A Biol Sci Med Sci*. 2002;57:B177–B188.
39. Chiba T, Yamaza H, Shimokawa I. Role of insulin and growth hormone/insulin-like growth factor-1 signaling in lifespan extension: rodent longevity models for studying aging and calorie restriction. *Curr Genomics*. 2007;8:423–428.

Eur J Nucl Med Mol Imaging (2013) 40:125–132
DOI 10.1007/s00259-012-2261-2

ORIGINAL ARTICLE

Comparison of the binding characteristics of [^{18}F]THK-523 and other amyloid imaging tracers to Alzheimer's disease pathology

Ryuichi Harada · Nobuyuki Okamura · Shozo Furumoto · Tetsuro Tago · Masahiro Maruyama · Makoto Higuchi · Takeo Yoshikawa · Hiroyuki Arai · Ren Iwata · Yukitsuka Kudo · Kazuhiko Yanai

Received: 1 May 2012 / Accepted: 21 September 2012 / Published online: 26 October 2012

Abstract
Purpose Extensive deposition of senile plaques and neurofibrillary tangles in the brain is a pathological hallmark of Alzheimer's disease (AD). Although several PET imaging agents have been developed for in vivo detection of senile plaques, no PET probe is currently available for selective detection of neurofibrillary tangles in the living human brain. Recently, [^{18}F]THK-523 was developed as a potential in vivo imaging probe for tau pathology. The purpose of this study was to compare the binding properties of [^{18}F]THK-523 and other amyloid imaging agents, including PiB, BF-227 and FDDNP, to synthetic protein fibrils and human brain tissue.
Methods In vitro radioligand binding assays were conducted using synthetic amyloid β_{42} and K18ΔK280-tau fibrils. Nonspecific binding was determined by the addition of unlabelled compounds at a concentration of 2 μM. To examine radioligand binding to neuropathological lesions, in vitro autoradiography was conducted using sections of AD brain.
Results [^{18}F]THK-523 showed higher affinity for tau fibrils than for Aβ fibrils, whereas the other probes showed a higher affinity for Aβ fibrils. The autoradiographic analysis indicated that [^{18}F]THK-523 accumulated in the regions containing a high density of tau protein deposits. Conversely, PiB and BF-227 accumulated in the regions containing a high density of Aβ plaques.
Conclusion These findings suggest that the unique binding profile of [^{18}F]THK-523 can be used to identify tau deposits in AD brain.

Keywords PET probes · Tau · Amyloid · Alzheimer's disease

Electronic supplementary material The online version of this article (doi:10.1007/s00259-012-2261-2) contains supplementary material, which is available to authorized users.

R. Harada · N. Okamura (✉) · S. Furumoto · T. Yoshikawa · K. Yanai
Department of Pharmacology,
Tohoku University School of Medicine,
2-1, Seiryo-machi, Aoba-ku,
Sendai 980-8575, Japan
e-mail: nookamura@med.tohoku.ac.jp

S. Furumoto · T. Tago · R. Iwata
Division of Radiopharmaceutical Chemistry,
Cyclotron and Radioisotope Center, Tohoku University,
Sendai, Japan

M. Maruyama · M. Higuchi
Molecular Imaging Center, National Institute
of Radiological Sciences,
Chiba, Japan

H. Arai
Department of Geriatrics and Gerontology, Institute of
Development, Aging and Cancer, Tohoku University,
Sendai, Japan

Y. Kudo
Innovation of New Biomedical Engineering Center,
Tohoku University,
Sendai, Japan

Introduction

Senile plaques and neurofibrillary tangles (NFTs) composed of amyloid-β (Aβ) peptides and aggregated tau proteins, respectively, are the pathological hallmarks of

Alzheimer's disease (AD). In vivo amyloid imaging techniques have received a lot of attention for their promise in presymptomatic detection of Aβ pathology [1]. Recently, several β-sheet binding radiotracers have been developed as PET amyloid imaging agents [2]. Among them, ^{18}F-labelled 2-(1-{6-[(2-fluoroethyl(methyl)amino)-2-naphthyl)ethylidene)malononitrile ([^{18}F]FDDNP) was the first PET probe to be applied to clinical PET imaging in patients with AD [3]. This tracer demonstrated higher regional uptake in the medial temporal lobe and neocortex, and was claimed to bind to Aβ and tau pathological lesions [3]. Subsequently, ^{11}C-labelled 2-[4′-(methylamino)phenyl]-6-hydroxybenzothiazole ([^{11}C]PiB) and 2-(2-[dimethylaminothiazole-5-yl]ethenyl)-6-(2-[fluoro]ethoxy)benzoxazole ([^{11}C]BF-227) were also developed as amyloid imaging radiotracers. These tracers bind to Aβ fibrils with high affinity [4] and have demonstrated a significantly higher retention in the neocortical areas of brains of AD patients than of healthy controls [5, 6]. Furthermore, post-mortem analysis of AD patients who had undergone [^{11}C]PiB PET imaging before death suggested a strong correlation between in vivo PiB binding and regional distribution of Aβ plaques [7].

Amyloid imaging with PET can detect AD pathology in its preclinical stage [8]. However, amyloid deposition as assessed by [^{11}C]PiB PET correlates poorly with cognitive impairment in AD [9, 10], whereas deposition of tau in the medial temporal cortex is closely associated with neuronal death in this region. Selective tau imaging would provide important information about the tau pathophysiological features in AD, allowing correlation of brain tau load with cognitive decline, monitoring of disease progression and evaluation of therapeutic efficacy of newly developed therapies. Potential candidates for in vivo tau imaging agents include quinoline derivatives [11], and in a recent study, we found that one quinoline derivative, [^{18}F]THK-523, showed higher affinity for tau rather than amyloid fibrils. Furthermore, an autoradiography analysis indicated that this tracer binds specifically to tau deposits but not Aβ burden at tracer concentrations usually achieved during a PET scan [12].

The binding profiles of PiB, BF-227 and FDDNP to Aβ fibrils have been well described. Because tau, α-synuclein and prion fibrils, as well as Aβ fibrils, share a common β-sheet secondary structure, these compounds can potentially bind all these misfolded proteins. A previous study indicated that PiB binds to both Aβ and PHF tau pathology in vitro [13]. However, the binding occurs at higher concentrations than usually achieved in vivo during a PET scan. Furthermore, PET–pathology correlation studies have demonstrated that PiB binding reflects Aβ pathology [7, 14]. Newly developed ^{18}F-labelled amyloid PET tracers have similarly shown good correlation with Aβ plaque density [15, 16]. However, the binding affinity of these radiotracers for tau fibrils remains unknown and the binding properties of [^{18}F]THK-523 have not been directly compared with those of other amyloid PET agents. Here, we compared the binding affinity of [^{18}F]THK-523 to synthetic Aβ and tau protein fibrils as well as to senile plaques and NFTs in human brain samples with those of PiB, BF-227 and FDDNP, to characterize the binding properties of THK-523 and to obtain a better understanding of current and future PET data.

Materials and methods

Materials

The nonlabelled compounds PiB, BF-227, FDDNP, THK-523 (Fig. 1) and their precursors were custom-synthesized by Tanabe R&D Service (Osaka, Japan). Human $A\beta_{42}$ was purchased from Peptide Institute Inc. (Mino, Japan). Recombinant K18ΔK280-tau protein was obtained from Invitrogen (Tokyo, Japan).

Radiolabelling of PiB, BF-227, THK-523 and FDDNP

[^{3}H]PiB (specific activity 2.96 GBq/μmol) was purchased from American Radiolabeled Chemicals (St. Louis, MO). [^{11}C]PiB was radiolabelled using its precursor (2-(4-aminophenyl)-6-methoxymethoxybenzothiazole) and [^{11}C]methyl triflate, as

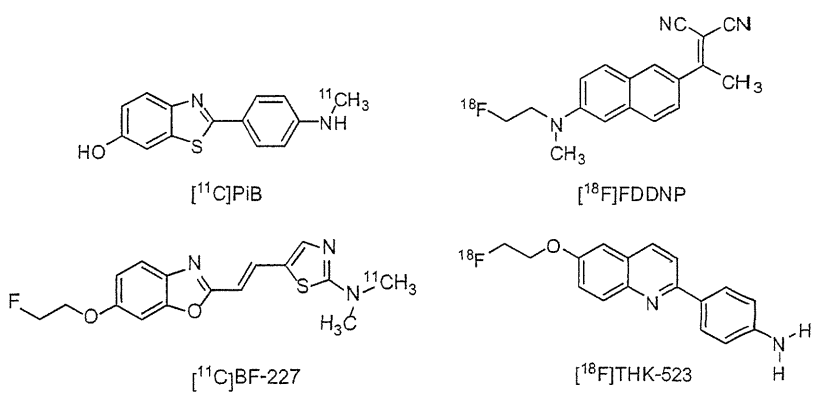

Fig. 1 Chemical structures of [^{11}C]PiB, [^{18}F]FDDNP, [^{11}C]BF-227 and [^{18}F]THK-523

previously described [17, 18]. The mean specific activity of [^{11}C]PiB was 34.6 GBq/μmol.

[^{18}F]BF-227 was synthesized by nucleophilic substitution of the tosylate precursor (2-[2-(2-dimethylaminothiazol-5-yl)ethenyl]-6-[2-(tosyloxy)ethoxy]benzoxazole. After a 10-min reaction at 110 °C, the crude mixture was partially purified on an activated Sep-Pak tC18 cartridge before being purified by semi-preparative reverse-phase HPLC. Standard tC18 Sep-Pak reformulation produced [^{18}F]BF-227 in >95 % purity. The radiochemical yield was 12–19 % (non-decay-corrected), and the mean specific activity of [^{18}F]BF-227 was 163 GBq/μmol at the end of the synthesis. [^{11}C]BF-227 was synthesized using *N*-desmethylated derivatives as its precursor and [^{11}C]methyl triflate, as previously described [6]. The mean specific activity of [^{11}C]BF-227 was 136 GBq/μmol.

[^{18}F]THK-523 was synthesized by nucleophilic substitution of the tosylate precursor (2-(4-aminophenyl)-6-(2-tosyloxyethoxy)quinolone) as previously described [12]. The standard tC18 Sep-Pak reformulation produced [^{18}F]THK-523 in >95 % purity. The radiochemical yield was 38–49 % (non-decay-corrected), and the mean specific activity of [^{18}F]THK-523 was 68 GBq/μmol at the end of the synthesis.

[^{18}F]FDDNP was radiolabelled by the nucleophilic substitution of the tosylate precursor (2-{[6-(2,2-dicyano-1-methylvinyl)-2-naphthyl](methyl)amino}ethyl-4-methylbenzenesulphonate) as previously described [19]. After a 15-min reaction at 95 °C, the crude mixture was partially purified on an activated Sep-Pak tC18 cartridge before being purified by semipreparative reverse-phase HPLC. Standard tC18 Sep-Pak reformulation produced [^{18}F]FDDNP in >95 % purity. The radiochemical yield was 12–19 % (non-decay-corrected), and the mean specific activity of [^{18}F]FDDNP was 27 GBq/μmol at the end of the synthesis. All analysis HPLC chromatograms are shown in the Supplementary figure.

In vitro radioligand binding assays

Synthetic $A\beta_{42}$ fibrils and K18ΔK280-tau fibrils were prepared as previously described [12]. For in vitro binding assays, synthetic $A\beta_{42}$ or K18ΔK280 fibrils (200 nM) were incubated with increasing concentrations of [^{3}H]PiB and ^{18}F-labelled compounds (0.5–200 nM). To account for nonspecific binding of [^{3}H]PiB and ^{18}F-labelled compounds, the above-mentioned reactions were performed in triplicate in the presence of each unlabelled compound at a concentration of 2 μM.

The binding reactions were incubated for 1 h for the ^{18}F-labelled compounds and 3 h for [^{3}H]PiB at room temperature, in 200 μL of assay buffer (Dulbecco's PBS, 0.1 % BSA). Separation of bound from free radioactivity was achieved by filtration under reduced pressure (MultiScreen HTS Vacuum Manifold, MultiScreen HTS 96-well 0.65-μm filtration plate; Millipore, Billerica, MA). The filters were washed three times with 200-μL assay buffer, and the filters containing the bound ^{18}F-labelled compounds were then assayed for radioactivity in a γ counter (AccuFLEX γ7000, Aloka, Tokyo, Japan). The filters containing [^{3}H]PiB were incubated in 2 mL of scintillation fluid (Aquasol-2; PerkinElmer, Boston, MA), and the radioactivity of ^{3}H was counted using a β counter (LS6500 liquid scintillation counter; Beckman Coulter, Brea, CA). The binding data were analysed with curve-fitting software that calculated the K_D and B_{max} using nonlinear regression (GraphPad Prism version 5.0; GraphPad Software, San Diego, CA).

Autoradiography, immunohistochemistry and Gallyas silver staining

Demographics of post-mortem brain samples are shown in Table 1. The frontal and medial temporal brain sections (6 μm thick) of three AD patients were incubated with 1.0 MBq/mL ^{11}C-labelled and ^{18}F-labelled compounds at room temperature for 10 min and then washed briefly with water and 50 % ethanol. After drying, the labelled sections were exposed to a BAS-III imaging plate (Fuji Film, Tokyo, Japan) overnight. The autoradiographic images were obtained using a BAS-5000 phosphoimaging instrument (Fuji Film) with a spatial resolution of 25×25 μm. The adjacent sections were immunostained using AT8 anti-tau monoclonal antibody (diluted 1:20; Innogenetics, Ghent, Belgium) and 6F/3D (diluted 1:50; Dako, Glostrup, Denmark). The adjacent sections were also stained by the Gallyas-Braak method, which has been reported to be NFT-specific [20].

Results

Binding affinity for synthetic Aβ and tau fibrils

To characterize the binding properties of THK-523, PiB, BF-227 and FDDNP, in vitro radioligand binding assays for synthetic $A\beta_{42}$ and truncated tau construct (K18ΔK280) fibrils were performed under the same experimental conditions. Truncated tau construct (K18ΔK280) consists of the four repeat regions (244–372) but lacking lysine 280 (ΔK280) observed in FTLD-17 familial mutation.

Table 1 Demographics of brain samples used in this study

Brain no.	Age (years)	Sex	Post-mortem interval (h)
AD1	76	F	16
AD2	82	F	17
AD3	92	F	8.5

K18ΔK280 tau aggregates exhibit the similar characteristic as PHF-tau from AD brain [21]. In addition, K18ΔK280 tau forms aggregates quickly without cofactor such as heparin [22]. Thus, we used K18ΔK280 fibrils for the in vitro binding assays. Our analysis indicated that [^{18}F]THK-523 had a higher binding affinity for tau fibrils (K_{D1} = 1.99 ± 0.21 nM, B_{max1} = 1.22 ± 0.24 pmol THK-523/nmol K18ΔK280-tau) than for $A\beta_{42}$ fibrils (K_{D1} = 30.3 ± 3.91 nM, B_{max1} = 12.6 ± 0.45 pmol THK-523/nmol $A\beta_{42}$), which was similar to previously published data [12]. On the other hand, [^{3}H]PiB bound to $A\beta_{42}$ fibrils with high affinity (K_{D1} = 0.84 ± 0.18 nM, B_{max1} = 0.44 ± 0.07 pmol PiB/nmol $A\beta_{42}$). [^{3}H]PiB also showed two binding sites for K18ΔK280-tau fibrils, but with a lower affinity (K_{D1} = 6.39 ± 1.63 nM, B_{max1} = 1.38 ± 0.48 pmol PiB/nmol K18ΔK280) than [^{18}F]THK-523. [^{18}F]BF-227 showed a high binding affinity for $A\beta_{42}$ fibrils (K_{D1} = 1.72 ± 0.83 nM, B_{max1} = 0.50 ± 0.14 pmol BF-227/nmol $A\beta_{42}$), similar to our previous report [23], but showed a lower affinity for tau fibrils (K_D = 30.2 ± 2.29 nM, B_{max} = 10.7 ± 0.24 pmol BF-227/nmol K18ΔK280-tau). [^{18}F]BF-227 had an approximately 20-fold higher affinity for the first class of $A\beta_{42}$ binding sites compared with tau fibrils. Only one class of [^{18}F]FDDNP binding site was identified on the $A\beta_{42}$ (K_D = 5.52 ± 1.97 nM, B_{max} = 0.277 ± 0.06 pmol FDDNP/nmol $A\beta_{42}$) and K18ΔK280 tau fibrils (K_D = 36.7 ± 11.6 nM, B_{max} = 2.14 ± 0.46 pmol FDDNP/nmol K18ΔK280-tau). These results suggest that [^{18}F]FDDNP binds $A\beta_{42}$ fibrils with lower affinity than [^{3}H]PiB and [^{18}F]BF-227. Furthermore, [^{18}F]FDDNP had an approximately sevenfold higher affinity for $A\beta_{42}$ fibrils than for tau fibrils. These binding profiles are significantly different from that of [^{18}F]THK-523 (Table 2).

In vitro autoradiography of human brain sections

To further assess the binding selectivity of [^{18}F]THK-523, autoradiographic images of the frontal (Fig. 2) and medial temporal (Fig. 3) brain sections from three AD patients, using [^{18}F]THK-523, [^{11}C]PiB and [^{11}C]BF-227, were compared. While Aβ plaques in the frontal grey matter were labelled with [^{11}C]PiB (Fig. 2a–c) and [^{11}C]BF-227 (Fig. 2g–i), the binding of [^{18}F]THK-523 in the frontal grey matter (Fig. 2m–o) was considerably lower. In the medial temporal brain sections, [^{11}C]PiB (Fig. 3a–c) and [^{11}C]BF-227 (Fig. 3g–i) did not accumulate in the hippocampal CA1 area, whereas [^{18}F]THK-523 (Fig. 3m–o) did accumulate in this area (Fig. 3m–o). The presence of a high density of tau and a low density of Aβ in this area was confirmed by immunohistochemistry (Fig. 3d–f, j–l). Furthermore, the band-like distribution of [^{18}F]THK-523 in the inner layer of the temporal grey matter was similar to the distribution of tau (Fig. 3j–l). In the high-magnification images of case AD3 (Fig. 3p–v), the distribution of [^{18}F]THK-523 closely resembled Gallyas silver staining and tau immunostaining. [^{18}F]THK-523 binding was observed in the areas showing a high density of NFTs in the hippocampal CA1, the layer pre-α and pri-α in the entorhinal cortex (ERC) (Fig. 3p, q, r, t). Intriguingly, [^{18}F]THK-523 labelling in the layer pre-α of the ERC corresponded to Gallyas silver staining better than tau immunostaining, suggesting the preferential binding of [^{18}F]THK-523 to extracellular tau deposits that were clearly visualized by Gallyas silver staining [25]. In contrast to [^{18}F]THK-523, the distribution of [^{11}C]PiB was similar to that of Aβ immunohistochemistry (Fig 3q, u, v). [^{11}C]PiB binding corresponded to the formation of amyloid in the parvopyramidal layer of the presubicular area and in the layers pre-β and pre-γ of the ERC (Fig. 3s, v) [26].

Discussion

In the study reported here, we for the first time directly compared the binding properties of the novel quinoline derivative THK-523 and other amyloid PET probes. Our data suggest the potential utility of THK-523 for the selective detection of PHF-tau in the living human brain, which has not previously been achieved. The autoradiographic images of sections from AD brains revealed that [^{18}F]THK-523 successfully labelled PHF-tau deposits but did not label Aβ deposits in the frontal and temporal cortices. These findings suggest that [^{18}F]THK-523 is a promising

Table 2 K_D and B_{max} values of [^{3}H]PiB, [^{18}F]BF-227, [^{18}F]FDDNP and [^{18}F]THK-523 for K18ΔK280-tau and $A\beta_{42}$ fibrils

Compound	K18ΔK280 fibrils				$A\beta_{42}$ fibrils			
	K_{D1}	B_{max1}	K_{D2}	B_{max2}	K_{D1}	B_{max1}	K_{D2}	B_{max2}
[^{18}F]THK-523	1.99±0.21	1.22±0.24	50.7±2.73	4.55±0.74	30.3±3.91	12.6±0.45	–	–
[^{18}F]BF-227	30.2±2.29	10.7±0.24	–	–	1.72±0.83	0.50±0.14	56.1±25.1	13.4±4.37
[^{18}F]FDDNP	36.7±11.6	2.14±0.46	–	–	5.52±1.97	0.277±0.06	–	–
[^{3}H]PiB	6.39±1.63	1.38±0.48	304±77.4	20.6±11.2	0.84±0.18	0.44±0.07	60.6±8.32	26.1±8.57

K_D values are in nanomoles, and B_{max} values are in picomoles compound per nanomole fibrils (n=3).

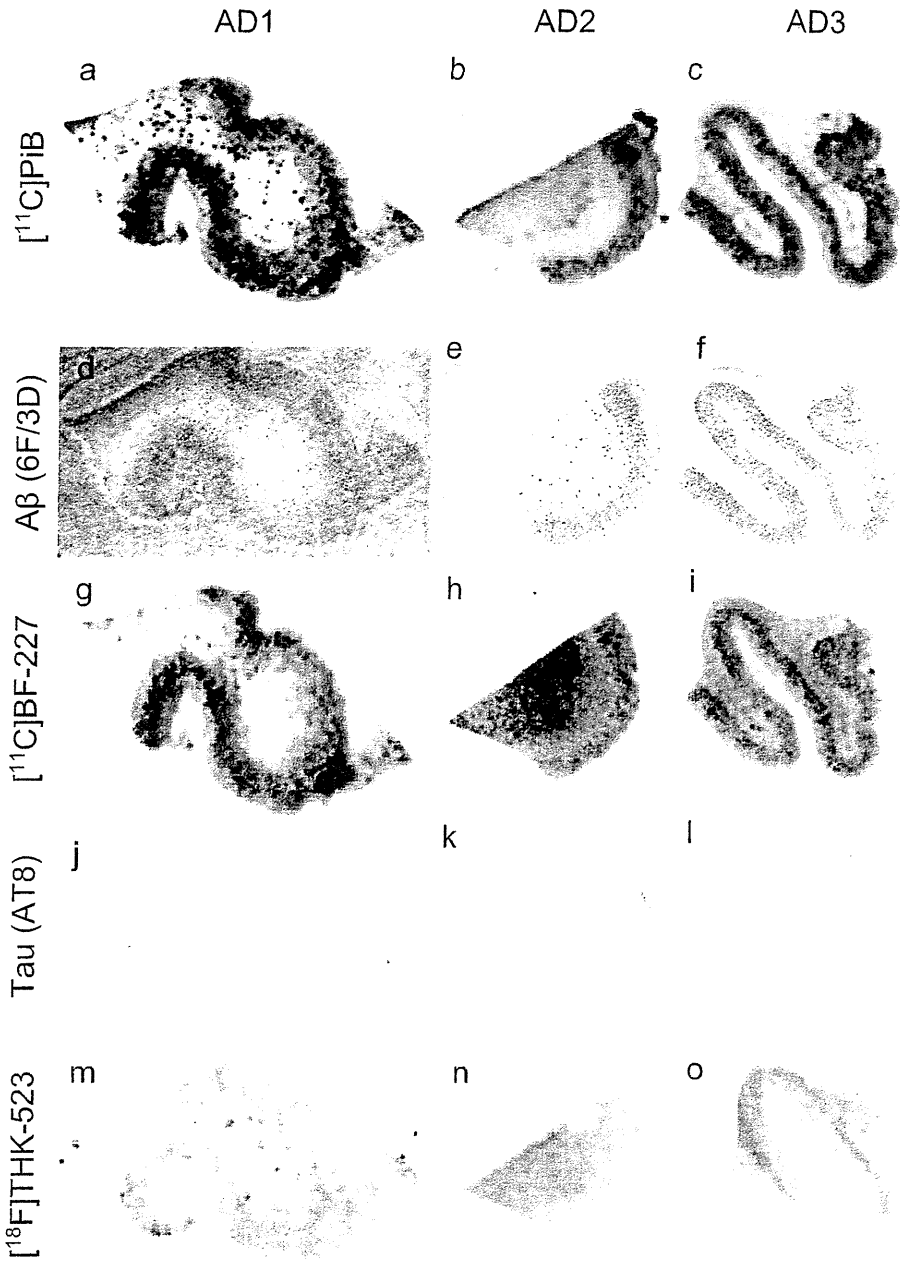

Fig. 2 Comparison of [^{11}C]PiB, [^{11}C]BF-227 and [^{18}F]*THK-523 autoradiography* with the Aβ and tau immunostaining in sections of the frontal brain from three patients with AD (*AD1*, *AD2*, *AD3*). Both [^{11}C]PiB (**a–c**) and [^{11}C]BF-227 (**g–i**) showed dense accumulation in the grey matter, closely resembling the pattern of Aβ immunohistochemistry using the 6F/3D antibody (**d–f**). [^{18}F]*THK-523* (**m–o**) *did not* accumulate in the grey matter, which was correlated with no marked staining with anti-tau antibody AT8 (**j–l**)

candidate as a tau imaging tracer, and could also be a lead compound for future development of tau-selective radiotracers. We speculate that [^{18}F]THK-523 would show retention in tau-rich brain regions if administered to AD patients. However, the specific signal of [^{18}F]THK-523 might be lower than those of PiB and BF-227 owing to the lower amount of tau deposits in the neocortex of AD patients [27]. Further compound optimization may be required to achieve higher contrast imaging of PHF-tau deposits.

In in vitro saturation binding studies [^{18}F]THK-523 bound with higher affinity to tau fibrils (K_{D1} 1.99 nM) than to $A\beta_{42}$ fibrils (K_{D1} 30.3 nM), whereas PiB and BF-227 showed the opposite binding characteristics. [^{3}H]PiB bound with higher affinity to $A\beta_{42}$ fibrils (K_{D1} 0.84 nM) than to tau fibrils (K_{D1} 6.39 nM), similar to previous reports [7, 28, 29], and [^{18}F]BF-227 had more than a tenfold higher affinity for $A\beta_{42}$ fibrils (K_{D1} 1.72 nM) than for tau fibrils (K18ΔK280; K_{D1} 30.2 nM). Autoradiographic images of sections of AD brain revealed that [^{11}C]PiB and [^{11}C]BF-227 accumulated in the grey matter of the neocortex, which closely resembled the staining pattern of Aβ immunohistochemistry. A previous study suggested that [^{3}H]PiB labelled NFTs at tracer concentrations usually achieved during a PET scan [13]. However, another study showed no binding of the PiB derivative [^{3}H]BTA-1 to

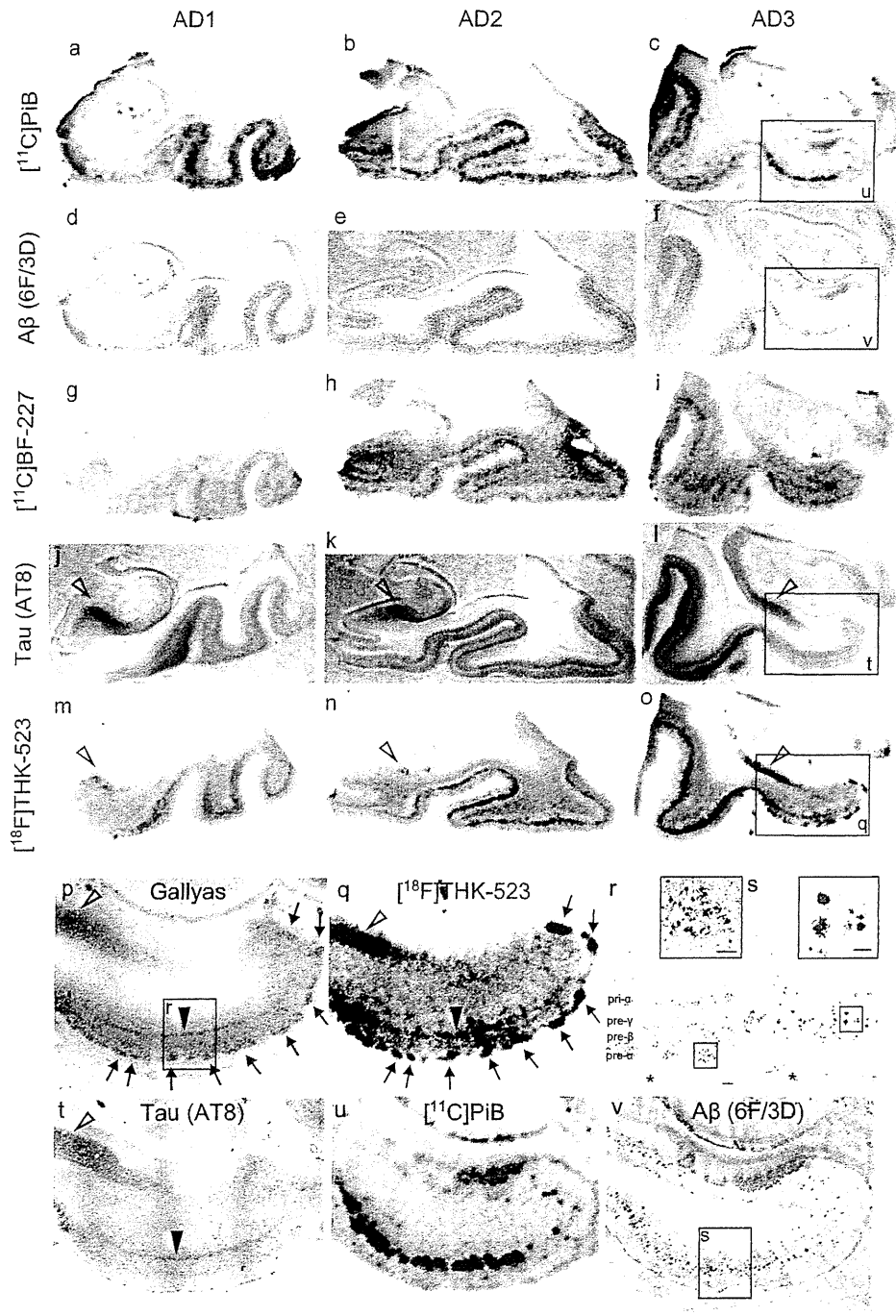

Fig. 3 Comparison of [^{11}C]PiB, [^{11}C]BF-227 and [^{18}F]THK-523 autoradiography with Aβ and tau immunostaining images in sections of the medial temporal brain from three patients with AD (*AD1*, *AD2*, *AD3*). [^{11}C]PiB (**a–c**) and [^{11}C]BF-227 (**g–i**) do not accumulate in the hippocampal CA1 area which contains a low density of Aβ (**d–f**). In contrast, accumulation of [^{18}F]THK-523 is observed in the hippocampal CA1 area (**m–o**, *arrowheads*), which closely resembles AT8 immunoreactivity (**j–l**, *arrowheads*). In addition, the band-like labelling pattern of [^{18}F]THK-523 in the inner layer of temporal cortex (**m–o**) is closely similar to that of AT8 immunostaining (**j–l**). **p–v** High magnification images of the medial temporal sections from patient AD3. Many clusters of [^{18}F]THK-523 binding in the ERC are consistent with Gallyas silver staining (**p**, **q**, *arrows*). **r** Close-up image from **p**. Numerous NFTs are located in the layer pre-α of the ERC (**r** *inset*). The band-like distribution of [^{18}F]THK-523 in the layer pri-α of the ERC also resembles the labelling pattern of Gallyas silver staining (**p**, *filled arrowhead*) as well as AT8 immunoreactivity (**t**, *filled arrowhead*). [^{11}C]PiB binding (**u**) is also present in the ERC, but obviously different from [^{18}F]THK-523 binding (**q**) and similar to the 6F/3D immunostaining pattern (**v**). Lake-like amyloid in the presubicular region (**v**) is labelled with [^{11}C]PiB, but not with [^{18}F]THK-523. **s** Close-up image from **v**. Aβ plaques (**s** *inset*) located in the layer pre-β and pre-γ are intensely labelled with [^{11}C]PiB (**u**). *Asterisks* in **r** and **s** denote the same large blood vessel. *Scale bar* 100 μm

plaque-free and NFT-rich ERC homogenates, despite the high amount of [^{3}H]BTA-1 binding to frontal cortex homogenates containing high levels of neuritic plaques [30]. Autoradiographic and immunohistochemical analyses indicated that PiB predominantly binds to senile plaques but not to NFTs. These findings are consistent with the findings from clinical PiB-PET studies showing no remarkable PiB retention in the medial temporal cortex of AD patients [7].

Another radiotracer, [^{18}F]FDDNP, has been reported to detect Aβ and tau pathological lesions in AD patients [3]. Previous clinical PET studies have shown higher cortical uptake of [^{18}F]FDDNP in the lateral and medial temporal lobes of AD subjects [3, 5]. Furthermore, a multitracer PET study of [^{11}C]PiB and [^{18}F]FDDNP has shown significant retention of FDDNP in the medial temporal cortex, albeit no remarkable retention of PiB in the same region [31]. However, in vitro binding studies have shown the limited binding affinity of [^{3}H]FDDNP to AD pathological lesions [24], and a previous autoradiographic analysis has suggested that [^{3}H]FDDNP does not significantly label any region in AD brain [24]. Previous in vitro binding studies additionally showed the binding affinity of FDDNP for $A\beta_{40}$ fibrils (K_D 0.12, 85 nM) [19, 24], but the binding affinity for tau fibrils was not reported. Here, we showed that the binding affinity of [^{18}F]FDDNP for tau fibrils (K_{D1} 36.7 nM) was similar to that of [^{18}F]BF-227 (K_{D1} 30.2 nM), but much higher than that of [^{18}F]THK-523 (K_{D1} 1.99 nM).

In conclusion, the binding profiles of [^{18}F]THK-523, [^{11}C]PiB, [^{18}F]BF-227, and [^{18}F]FDDNP were compared using in vitro saturation binding assays and autoradiography of sections of AD brain. These data suggest that [^{18}F]THK-523 shows a binding preference for tau protein fibrils. Therefore, [^{18}F]THK-523 is a candidate as a radiotracer to identify tau protein deposits and a lead compound for future tracer development. Ongoing clinical trials will clarify the clinical utility of this tracer and its derivatives for tau imaging in vivo.

Acknowledgments This study was supported by the Industrial Technology Research Grant Program of the NEDO in Japan, Health and Labor Sciences Research Grants from the Ministry of Health, Labor, and Welfare of Japan, and Grant-in-Aid for Scientific Research (B) (23390297).

References

1. Nordberg A, Rinne JO, Kadir A, Langstrom B. The use of PET in Alzheimer disease. Nat Rev Neurol. 2010;6:78–87. doi:10.1038/nrneurol.2009.217.
2. Furumoto S, Okamura N, Iwata R, Yanai K, Arai H, Kudo Y. Recent advances in the development of amyloid imaging agents. Curr Top Med Chem. 2007;7:1773–89.
3. Shoghi-Jadid K, Small GW, Agdeppa ED, Kepe V, Ercoli LM, Siddarth P, et al. Localization of neurofibrillary tangles and beta-amyloid plaques in the brains of living patients with Alzheimer disease. Am J Geriatr Psychiatry. 2002;10:24–35.
4. Mathis CA, Wang Y, Holt DP, Huang GF, Debnath ML, Klunk WE. Synthesis and evaluation of 11C-labeled 6-substituted 2-arylbenzothiazoles as amyloid imaging agents. J Med Chem. 2003;46:2740–54. doi:10.1021/jm030026b.
5. Klunk WE, Engler H, Nordberg A, Wang Y, Blomqvist G, Holt DP, et al. Imaging brain amyloid in Alzheimer's disease with Pittsburgh Compound-B. Ann Neurol. 2004;55:306–19. doi:10.1002/ana.20009.
6. Kudo Y, Okamura N, Furumoto S, Tashiro M, Furukawa K, Maruyama M, et al. 2-(2-[2-Dimethylaminothiazol-5-yl]ethenyl)-6- (2-[fluoro]ethoxy)benzoxazole: a novel PET agent for in vivo detection of dense amyloid plaques in Alzheimer's disease patients. J Nucl Med. 2007;48:553–61.
7. Ikonomovic MD, Klunk WE, Abrahamson EE, Mathis CA, Price JC, Tsopelas ND, et al. Post-mortem correlates of in vivo PiB-PET amyloid imaging in a typical case of Alzheimer's disease. Brain. 2008;131:1630–45. doi:10.1093/brain/awn016.
8. Sperling RA, Aisen PS, Beckett LA, Bennett DA, Craft S, Fagan AM, et al. Toward defining the preclinical stages of Alzheimer's disease: recommendations from the National Institute on Aging-Alzheimer's Association workgroups on diagnostic guidelines for Alzheimer's disease. Alzheimers Dement. 2011;7:280–92. doi:10.1016/j.jalz.2011.03.003.
9. Jack Jr CR, Knopman DS, Jagust WJ, Shaw LM, Aisen PS, Weiner MW, et al. Hypothetical model of dynamic biomarkers of the Alzheimer's pathological cascade. Lancet Neurol. 2010;9:119–28. doi:10.1016/S1474-4422(09)70299-6.
10. Pike KE, Savage G, Villemagne VL, Ng S, Moss SA, Maruff P, et al. Beta-amyloid imaging and memory in non-demented individuals: evidence for preclinical Alzheimer's disease. Brain. 2007;130:2837–44. doi:10.1093/brain/awm238.
11. Okamura N, Suemoto T, Furumoto S, Suzuki M, Shimadzu H, Akatsu H, et al. Quinoline and benzimidazole derivatives: candidate probes for in vivo imaging of tau pathology in Alzheimer's disease. J Neurosci. 2005;25:10857–62. doi:10.1523/JNEUROSCI.1738-05.2005.
12. Fodero-Tavoletti MT, Okamura N, Furumoto S, Mulligan RS, Connor AR, McLean CA, et al. 18F-THK523: a novel in vivo tau imaging ligand for Alzheimer's disease. Brain. 2011;134:1089–100. doi:10.1093/Brain/Awr038.
13. Lockhart A, Lamb JR, Osredkar T, Sue LI, Joyce JN, Ye L, et al. PIB is a non-specific imaging marker of amyloid-beta (Abeta) peptide-related cerebral amyloidosis. Brain. 2007;130:2607–15. doi:10.1093/brain/awm191.
14. Burack MA, Hartlein J, Flores HP, Taylor-Reinwald L, Perlmutter JS, Cairns NJ. In vivo amyloid imaging in autopsy-confirmed Parkinson disease with dementia. Neurology. 2010;74:77–84. doi:10.1212/WNL.0b013e3181c7da8e.
15. Clark CM, Schneider JA, Bedell BJ, Beach TG, Bilker WB, Mintun MA, et al. Use of florbetapir-PET for imaging beta-amyloid pathology. JAMA. 2011;305:275–83. doi:10.1001/jama.2010.2008.
16. Wong DF, Moghekar AR, Rigamonti D, Brasic JR, Rousset O, Willis W, et al. An in vivo evaluation of cerebral cortical amyloid with [(18)F]Flutemetamol using positron emission tomography compared with parietal biopsy samples in living normal pressure hydrocephalus patients. Mol Imaging Biol. 2012. doi:10.1007/s11307-012-0583-x.
17. Maeda J, Ji B, Irie T, Tomiyama T, Maruyama M, Okauchi T, et al. Longitudinal, quantitative assessment of amyloid, neuroinflammation, and anti-amyloid treatment in a living mouse model of Alzheimer's disease enabled by positron emission tomography. J Neurosci. 2007;27:10957–68. doi:10.1523/JNEUROSCI.0673-07.2007.

18. Manook A, Yousefi BH, Willuweit A, Platzer S, Reder S, Voss A, et al. Small-animal PET imaging of amyloid-beta plaques with [11C]PiB and its multi-modal validation in an APP/PS1 mouse model of Alzheimer's disease. PLoS One. 2012;7:e31310. doi:10.1371/journal.pone.0031310.
19. Agdeppa ED, Kepe V, Liu J, Flores-Torres S, Satyamurthy N, Petric A, et al. Binding characteristics of radiofluorinated 6-dialkylamino-2-naphthylethylidene derivatives as positron emission tomography imaging probes for beta-amyloid plaques in Alzheimer's disease. J Neurosci. 2001;21:RC189.
20. Gallyas F. Silver staining of Alzheimer's neurofibrillary changes by means of physical development. Acta Morphol Acad Sci Hung. 1971;19:1–8.
21. Barghorn S, Davies P, Mandelkow E. Tau paired helical filaments from Alzheimer's disease brain and assembled in vitro are based on beta-structure in the core domain. Biochemistry. 2004;43:1694–703. doi:10.1021/bi0357006.
22. von Bergen M, Barghorn S, Muller SA, Pickhardt M, Biernat J, Mandelkow EM, et al. The core of tau-paired helical filaments studied by scanning transmission electron microscopy and limited proteolysis. Biochemistry. 2006;45:6446–57. doi:10.1021/bi052530j.
23. Fodero-Tavoletti MT, Mulligan RS, Okamura N, Furumoto S, Rowe CC, Kudo Y, et al. In vitro characterisation of BF227 binding to alpha-synuclein/Lewy bodies. Eur J Pharmacol. 2009;617:54–8. doi:10.1016/j.ejphar.2009.06.042.
24. Thompson PW, Ye L, Morgenstern JL, Sue L, Beach TG, Judd DJ, et al. Interaction of the amyloid imaging tracer FDDNP with hallmark Alzheimer's disease pathologies. J Neurochem. 2009;109:623–30. doi:10.1111/j.1471-4159.2009.05996.x.
25. Braak E, Braak H, Mandelkow EM. A sequence of cytoskeleton changes related to the formation of neurofibrillary tangles and neuropil threads. Acta Neuropathol. 1994;87:554–67.
26. Thal DR, Rub U, Schultz C, Sassin I, Ghebremedhin E, Del Tredici K, et al. Sequence of Abeta-protein deposition in the human medial temporal lobe. J Neuropathol Exp Neurol. 2000;59:733–48.
27. Villemagne VL, Furumoto S, Fodero-Tavoletti M, Harada R, Mulligan RS, Kudo Y, et al. The challenges of tau imaging. Future Neurol. 2012;7:409–21. doi:10.2217/fnl.12.34.
28. Fodero-Tavoletti MT, Smith DP, McLean CA, Adlard PA, Barnham KJ, Foster LE, et al. In vitro characterization of Pittsburgh compound-B binding to Lewy bodies. J Neurosci. 2007;27:10365–71. doi:10.1523/JNEUROSCI.0630-07.2007.
29. Klunk WE, Lopresti BJ, Ikonomovic MD, Lefterov IM, Koldamova RP, Abrahamson EE, et al. Binding of the positron emission tomography tracer Pittsburgh compound-B reflects the amount of amyloid-beta in Alzheimer's disease brain but not in transgenic mouse brain. J Neurosci. 2005;25:10598–606. doi:10.1523/JNEUROSCI.2990-05.2005.
30. Klunk WE, Wang Y, Huang GF, Debnath ML, Holt DP, Shao L, et al. The binding of 2-(4'-methylaminophenyl)benzothiazole to post-mortem brain homogenates is dominated by the amyloid component. J Neurosci. 2003;23:2086–92.
31. Shin J, Lee SY, Kim SH, Kim YB, Cho SJ. Multitracer PET imaging of amyloid plaques and neurofibrillary tangles in Alzheimer's disease. Neuroimage. 2008;43:236–44. doi:10.1016/j.neuroimage.2008.07.022.

Geriatrics Gerontology — Medline Indexed

Geriatr Gerontol Int 2013; **13:** *215–221*

Brain accumulation of amyloid β protein visualized by positron emission tomography and BF-227 in Alzheimer's disease patients with or without diabetes mellitus

Naoki Tomita,[1] Katsutoshi Furukawa,[1] Nobuyuki Okamura,[3] Manabu Tashiro,[4] Kaori Une,[1] Shozo Furumoto,[3] Ren Iwata,[5] Kazuhiko Yanai,[3] Yukitsuka Kudo[2] and Hiroyuki Arai[1]

[1]Department of Geriatrics and Gerontology, Division of Brain Sciences, Institute of Development, Aging and Cancer, [2]Department of NeuroImaging Research, Innovation New Biomedical Engineering Center, Tohoku University, [3]Department of Pharmacology, Tohoku University Graduate School of Medicine, [4]Division of Cyclotron Nuclear Medicine, and [5]Division of Radiopharmaceutical Chemistry, Cyclotron and Radioisotope Center, Sendai, Miyagi, Japan

Aim: Although diabetes mellitus (DM) is considered to be one of the most consistent risks for developing dementia, it is not known if the pathology in dementia patients with DM is similar to or distinct from typical pathological features of Alzheimer's disease (AD). To discover the mechanism of developing dementia in AD patients with DM in a living state, we studied the distribution of amyloid β (Aβ) protein of diabetic AD patients.

Methods: To evaluate the accumulation of Aβ, we examined 14 normal controls, four diabetic patients with AD and 11 non-diabetic patients with AD by positron emission tomography (PET) using BF-227, a currently developed Aβ tracer.

Results: The analysis of PET images among the three groups showed an abundant aggregated Aβ accumulation in the cerebral cortex of both AD patients with and without DM. The extent and distributions of BF-227 accumulation in diabetic AD patients were not significantly different from these of non-diabetic AD patients.

Conclusion: These results suggest that the degree and extent of Aβ deposition is not significantly different between AD with DM and AD alone. **Geriatr Gerontol Int 2013; 13: 215–221.**

Keywords: Alzheimer's disease, amyloid β-peptides, diabetes mellitus, positron emission tomography.

Introduction

Long-standing lifestyle-related disorders from midlife, such as diabetes mellitus (DM) and hypertension, as well as obesity, are likely to be prominent risk factors for developing dementia and Alzheimer's disease (AD).[1] In fact, it is often found that diabetic patients develop AD in their later stage of life. Several separate community-based studies suggest that DM might increase the risk of dementia and AD,[2] though the underlying mechanisms are still not clearly explained.

Accepted for publication 9 April 2012.

Correspondence: Professor Hiroyuki Arai MD PhD, Department of Geriatrics and Gerontology, Division of Brain Sciences, Institute of Development, Aging and Cancer, Tohoku University, 4-1 Seiryomachi, Aobaku, Sendai 980-8498, Japan. Email: harai@idac.tohoku.ac.jp

AD is well characterized by an accumulation of misfolded proteins in the aging brain, which results in oxidative and inflammatory damage that in turn leads to energy failure and synaptic dysfunction.[3] In contrast, the impact of DM on the central nervous system (CNS) is not clearly understood.

Three major components related to type 2 DM that might underlie the effect of diabetes on the CNS in the development of AD are insulin resistance, hyperinsulinemia and hyperglycemia.[4] In addition to these three components, several other components are associated with the incidence of dementia or progression of cognitive decline. Whitmer *et al.* reported that severe hypoglycemic events were associated with a greater risk of dementia.[5] In addition, daily acute glucose fluctuations are also reported to be associated with cognitive decline.[6] Leptin, adiponectin and glucagon like peptide-1 (GLP-1) have recently been mentioned as potential factors that

are associated with the development of AD.[7–10] These components are not fully independent of each other, and it is unlikely that the impact of DM on the CNS depends exclusively on a single component. Which components play the major role might depend on the patient's clinical history and the present state of DM.

Each of these components are thought to act on several different pathways that are important in the pathophysiology of AD, either indirectly, through inflammation or the development of vascular disease, or directly, through effects on amyloid and tau metabolism, and the formation of advanced glycation end-products (AGE).[11] (Fig. 1)

Autopsy results in an epidemiological study concluded that macroscopic brain infarcts are more common in people with DM than those without the disorder, as well as microvascular changes.[12] In contrast, the reported incidence of Alzheimer's pathology in the brains of people with diabetes varies between studies. There are several contradictory papers reporting the relationship between DM and AD. Beeri *et al.* have reported that type 2 DM is inversely associated with AD pathology; that is, diabetic patients with dementia have a significantly lower density of senile plaques than non-diabetic patients with dementia.[13] Matsuzaki *et al.* reported that hyperinsulinemia and hyperglycemia caused by insulin resistance are positively associated with the pathology of AD.[14] In the autopsy population of the Honolulu-Asia Aging Study, the occurrence of neurofibrillary tangles and amyloid plaques in the hippocampus and cortex in people without the apolipoprotein E (*APOE*) ε4 allele were similar to those with and without DM. However, as for *APOE* ε4 carriers, these lesions were more common in people with DM than in people without DM.[12] It was also reported that DM is related to generating atherosclerosis and cerebral infarction, but not directly to AD pathology in diabetic patients with dementia.[15,16] Autopsy findings are usually a mixture of many changes occurring during the living state, so the findings do not necessarily reflect the changes that are clinically relevant.

Interaction between medication for DM, especially the effect of insulin use, and AD neuropathology should be considered as well, as the population of insulin users showed a much higher risk of developing dementia in a cohort study.[17] Biessels *et al.* showed significantly fewer amyloid plaques in diabetic patients who received both insulin and oral antidiabetic medication, as compared with diabetic patients with other medication statuses or non-diabetic subjects. The effects of diabetes medication were specific to amyloid plaques, as the extent of neurofibrillary tangles pathology was not associated with diabetes medications.[18] However, these findings are derived from autopsies, and it is not certain if the same results can be gained from living human brains.

Several neuroimaging studies reported that DM is a risk factor for silent and symptomatic brain infarcts seen with magnetic resonance imaging (MRI),[19,20] and DM is also associated with cortical and subcortical atrophy.[21–23] As functional imaging, it is well known that reductions in regional cerebral glucose metabolic rate (CMRglu), as measured by fludeoxyglucose F 18 positron emission tomography (FDG-PET), are associated with increased AD risk and can be observed years before the onset of dementia.[24,25] Baker *et al.* reported that insulin resistance in persons with normal cognition and prediabetes or early diabetes without treatment is associated with reductions in CMRglu measured with FDG-PET.[26] However, previous radiological studies had limitations on discussing the pathological mechanism, as the modalities used were not directly linked to Alzheimer's pathology. No studies have been carried out regarding a pathobiological link between DM and AD in living human subjects.

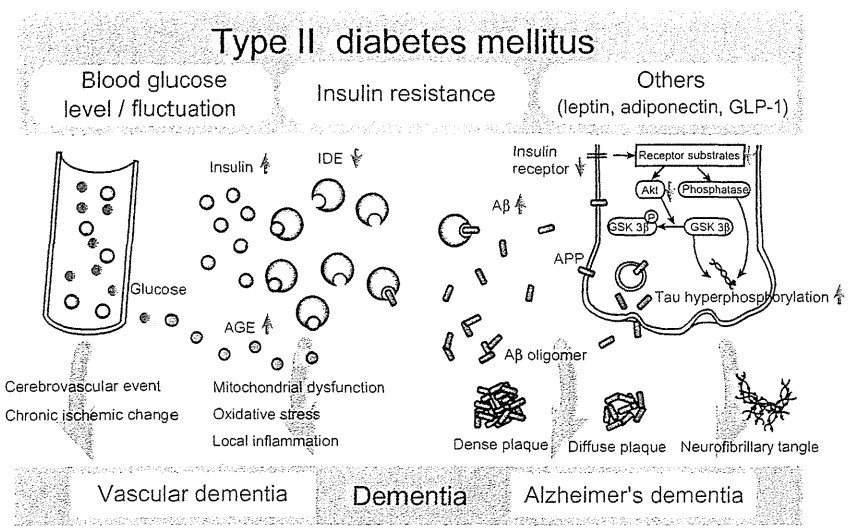

Figure 1 The possible pathological mechanisms associated with the impact of type 2 diabetes mellitus (DM) on the central nervous system (CNS). The major components of DM are described in the second column (only the three major components are described for easier understanding, though several other components are mentioned). Just below the column, the possible mechanism of developing dementia in type 2 DM. Aβ, amyloid β protein; AGE, advanced glycation end-products, APP, amyloid precursor protein; GLP-1, glucagon like peptide-1; GSK-3β, glycogen synthase kinase 3β; IDE, insulin degrading enzymes.

Table 1 Demographic data of the study participants

	Diagnostic group Normal control	AD alone	AD with DM
n	14	11	4
Sex (male/female)	7/7	4/7	2/2
Age	64.5 ± 2.9	78.5 ± 3.9	77.5 ± 5.2
MMSE	29.9 ± 0.1	20.5 ± 0.8	19.4 ± 2.8
ApoE ε4 allele (%)	0.12	0.35	0.37
HbA_{1c} (%)	5.7 ± 0.1	5.8 ± 0.1	7.2 ± 0.4

AD, Alzheimer's disease; DM, diabetes mellitus; HbA_{1c}, glycated hemoglobin; MMSE, Mini-Mental State Examination.

In order to clarify etiology and dementia subtypes in diabetic patients, we took a unique approach to visualize amyloid β protein (Aβ) deposition by positron emission tomography (PET) in living diabetic patients with dementia. The Aβ accumulation is successfully and non-invasively visualized by a recently-developed novel amyloid imaging probe called BF-227.[27–31] We used this tracer and applied it to "diabetic" and "non-diabetic" patients with clinically-diagnosed AD, to obtain more insights into differences in the extent and distribution of Aβ accumulation between diabetic and non-diabetic groups.

Methods

A total of 14 normal controls (NC), four diabetic patients with AD (AD with DM) and 11 non-diabetic patients with AD (AD alone) were examined. All the dementia patients were clinically diagnosed as probable AD according to the clinical criteria by "the National Institute of Neurological and Communicative Disorders and Stroke – Alzheimer's Disease and Related Disorders Association".[32] Brain MRI (1.5 Tesla; General Electric, Fairfield, CT, USA) was carried out on all the participants to exclude other causes of dementia. All the DM types of diabetic patients with AD were type 2. The study protocol was approved by the Committee on Clinical Investigation at Tohoku University School of Medicine and the Advisory Committee on Radioactive Substances at Tohoku University. After a complete description of the study to the patients and subjects, written informed consent was obtained.

The PET procedure using BF-227 is described elsewhere.[28,31] BF-227 and its *N*-desmethylated derivative (a precursor of [^{11}C]BF-227) were custom-synthesized by Tanabe R&D Service (Osaka, Japan) [^{11}C]BF-227 was synthesized from the precursor by *N*-methylation in dimethyl sulfoxide using [^{11}C]methyl triflate. The [^{11}C]BF-227 PET study was carried out using a PET SET-2400W scanner (Shimadzu, Kyoto, Japan). After intravenous injection of 211–366 mBq of [^{11}C]BF-227, dynamic PET images were obtained for 60 min with each subject's eyes closed. Standardized uptake value (SUV) images of [^{11}C]BF-227 were obtained by normalizing tissue radioactivity concentration by injected dose and bodyweight. Regions of interest (ROI) were placed on individual axial MR images in the cerebellar hemisphere, striatum, frontal, lateral temporal, medial temporal, parietal, occipital, anterior and posterior cingulate cortices. The ROI information was then copied onto dynamic PET SUV images, and regional SUV were sampled using Dr.View/LINUX software (AJS, Tokyo, Japan). Because there were neither senile plaques nor glucose hypometabolism in the cerebellum of AD patients, the ratios of regional SUV to cerebellar SUV (SUVR) were calculated as an index of [^{11}C]BF-227 retention. Neocortical SUVR was calculated by averaging SUVR in the frontal, lateral temporal, parietal and posterior cingulate cortices. Apolipoprotein E genotyping was carried out as previously described.[33]

The difference of Neocortex SUVR between the group of AD with DM and other groups was assessed with Student's *t*-test. The performance of diagnostic indices to discriminate among groups was assessed using receiver operating characteristic (ROC) analysis. Areas under ROC curves (AUC) were calculated and compared using GraphPad Prism Software (GraphPad Software, San Diego, CA, USA). Statistical significance was defined as $P < 0.05$.

Results

The clinical features of the three groups, NC, AD alone and AD with DM, are described in Table 1. Severities of dementia assessed by Mini-Mental State Examination were not significantly different between AD alone and AD with DM. Three patients were treated with only oral DM medications (patient A glimepiride + pioglitazone; patient B glimepiride + metformin + voglibose; patient

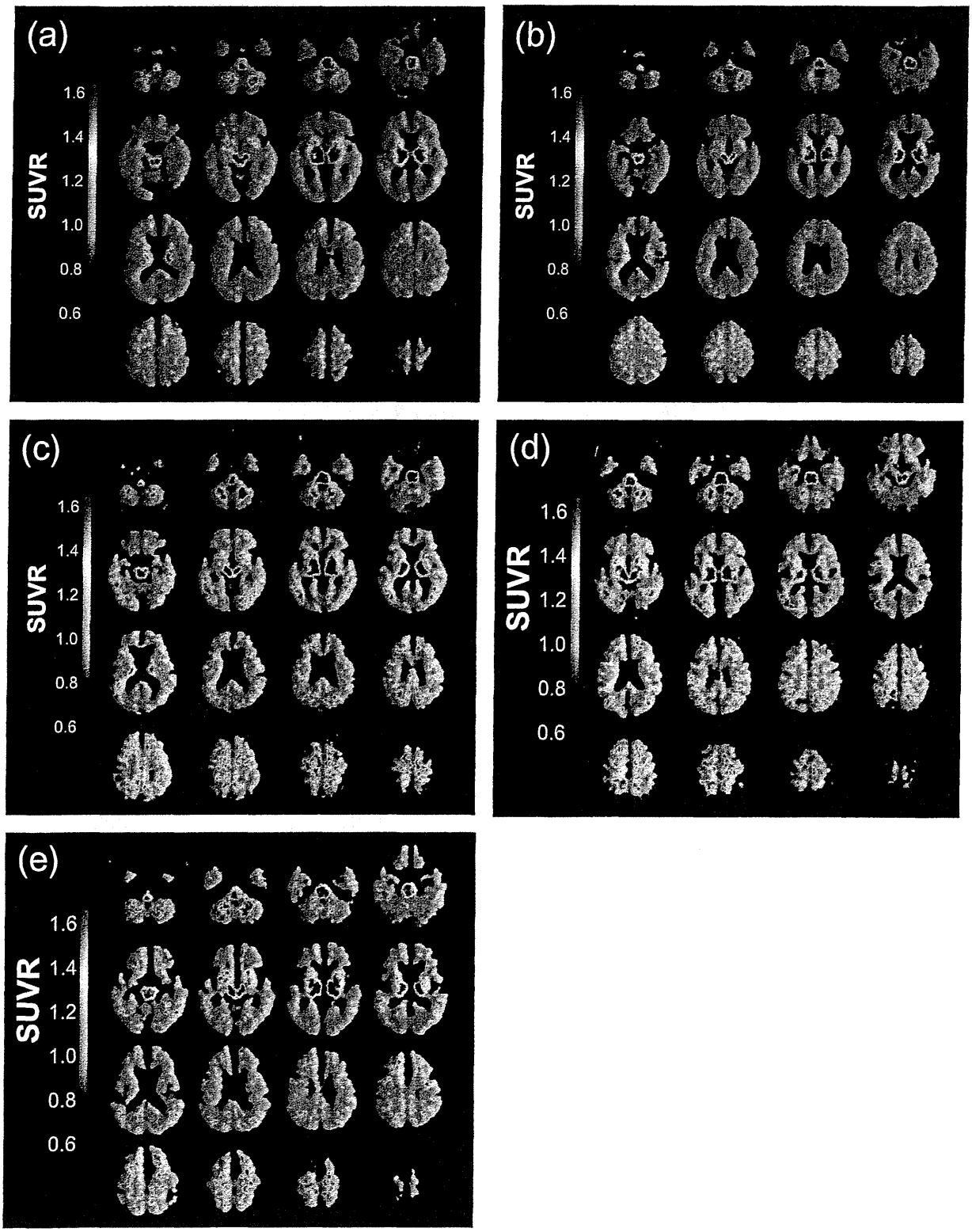

Figure 2 Representative BF-227 positron emission tomography images of each diagnostic group. (a) Normal control without diabetes mellitus (DM; 67-years-old, male, no complication; neocortical ratios of regional standardized uptake value to cerebellar standard uptake value ratio [SUVR] = 1.122). (b) Normal control with diabetes mellitus (67-years-old, female, insulin user; neocortical SUVR = 1.012). (c) Alzheimer's disease (AD) alone (75-years-old, female; neocortical SUVR = 1.230). (d) AD with DM (79-years-old, female, insulin user; neocortical SUVR = 1.240). (e) AD with DM (78-years-old, male, non-insulin user; SUVR = 1.18).

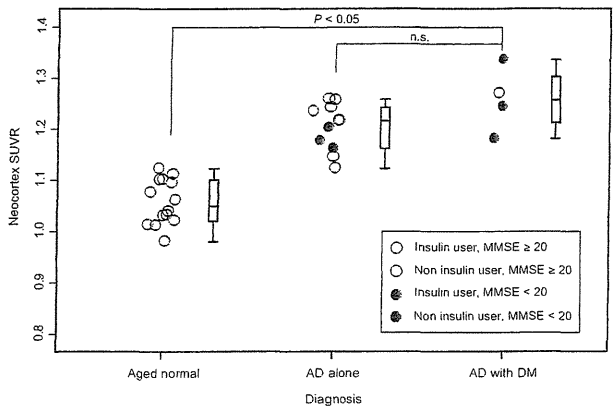

Figure 3 Box and scatter plots of ratios of regional standardized uptake value to cerebellar standard uptake value ration (SUVR) values with BF-227 in aged normal, Alzheimer's disease (AD) alone and AD with diabetes mellitus (DM) participants. Each circle indicates the mean SUVR from the mean neocortex. Red colored circle represents insulin user, whereas blue colored circle represents non-insulin user. There are no DM patients in the aged normal group shown with the blue circle. The filled circle represents the participants with Mini-Mental State Examination score less than 20. Although both AD with DM and AD alone showed significantly higher SUVR than the normal control group ($P < 0.05$), the difference between AD with DM and AD alone was not significant (n.s.).

Table 2 Characteristics of insulin users

	Subject 1 (no. 4) (normal cognition)	Subject 2 (no. 6) (AD patients)
Age	67	79
Sex	Female	Female
MMSE	28	21
ApoE genotype	3/3	3/3
CSF total tau (pg/ml)	–	334
BMI	24.7	19.8
HbA_{1c} (%)	7.6	8.2
Medication	Insulin only	Insulin, metformin
Hypoglycemic event	several	none
Duration of insulin use (years)	11	7

AD, Alzheimer's disease; BMI, body mass index; CSF, cerebrospinal fluid; HbA_{1c}, glycated hemoglobin; MMSE, Mini-Mental State Examination.

C metformin + voglibose), whereas only one AD with DM patient used insulin in addition to metformin. One DM patient was present in the normal control group. This patient in the control group had no oral medication. Insulin injection was the only medication.

MRI scans showed no or very few ischemic or hemorrhagic lesions observed in any of the participants. These small lesions were not strategic. White matter lesions (both periventricular and deep white matter) are all less than mild according to the Fazekas criteria (data not shown).[34]

After we obtained demographic information, we analyzed PET images with BF-227 among the three groups, and representative brain PET images are shown in Figure 2. As indicated in the figure, both the patients with AD alone and AD with DM showed significantly more robust retention of BF-227 than NC. Statistical analysis showed a significantly higher SUV-R of BF-227 ($P < 0.05$) in the cerebral cortex of AD alone and AD with DM than NC, as shown in Figure 3. Neocortical SUV-R of BF-227 in AD alone and AD with DM are not significantly different. Both the patients with AD alone and AD with DM showed increased BF-227 uptake in frontal, temporal, parietal, occipital and cingulated gyrus. The pattern of uptake was similar between the DM patients with insulin use and those without the use of insulin (Fig. 2). A similar pattern of uptake between insulin users and non-insulin users was seen both in the control group and the AD with DM group.

The clinical profiles of the two insulin users are shown in Table 2.

Discussion

The present study had two major findings. First, the uptake of BF-227 was significantly higher in both AD groups than that of the normal control group, regardless of DM complication. Second, the amount and pattern of the uptake was not affected by the use of insulin, both in the control group and the AD with DM group.

The first result that the severity and extent of the deposition did not differ significantly between the two groups suggests that both AD with DM and AD alone have robust deposition of senile plaques or typical AD pathology. In addition, all the participants we examined showed no or very few vascular lesions observed with MRI, indicating that we could exclude vascular dementia. The present result showed that the cause of developing dementia in DM patients cannot be fully explained by vascular mechanism. From the results of previous studies,[13,14] we assumed that either extra or less deposition of amyloid plaques would be seen in the brain of AD patients with DM complication. However, the brains of AD patients with DM showed a similar pattern and severity of the amyloid deposition to that seen in the brains of AD without DM complication. One possible explanation is that some kinds of protein that cannot be detected by BF-227 play a more important role than the classical aggregated plaque. Soluble

Aβ oligomers, which cannot be detected by BF-227, were shown to lower insulin receptor responses to insulin and cause substantial loss of neuronal surface insulin receptors.[35] Another possibility is that the additional effect of DM complication appears mainly through the increase in phosphorylation of tau, instead of an increase of Aβ plaque.

The second result of AD patients is in conflict with those reported by Beeri *et al.*[18] According to their conclusion, the AD patient with insulin and metformin use (subject 4 in Fig. 2) should have shown fewer senile plaques (lower uptake) as compared with diabetic patients with other medication status or non-diabetic subjects. One explanation for this inconsistency is that he/she was an *APOE* ε4 non-carrier. The occurrence of neurofibrillary tangles and amyloid plaques in people without the *APOE* ε4 allele were similar to those with and without DM in the autopsy population of the Honolulu-Asia Aging Study.[12] It is assumed that the effect of insulin and other medication use on reducing the plaques might only be effective in reducing the extra deposition of amyloid plaques in *APOE* ε4 carriers.

It was also found that the insulin user with normal cognition (subject 2 in Fig. 2) showed no difference in uptake. This subject was not obese, and started insulin injections 11 years before she undertook the PET procedure. Her glycohemoglobin level was 7.6%, and she had experienced several hypoglycemic events just before participation in the present study. From these clinical features, we assume that one of the main components of her DM were fluctuations of her blood glucose level (hyperglycemia and hypoglycemia). The interaction with ApoE ε4 might also be thought to be an explanation.

A limitation of the present study was that we could not adjust some factors, such as age, due to the small sample size. Because of the small sample size, the present study should be treated as a preliminary report. In addition, we could not measure the value of their homeostasis model assessment ratio, which is one of the key indicators of insulin resistance. We could not measure this indicator of insulin users, because they already had started insulin before admission to our clinic. Further studies are required to clarify the present report.

In conclusion, the present study provided new and important preliminary findings that a similar pathomechanism, which is the deposition of robust aggregated Aβ in the brain, is shared in both AD with DM and AD alone.

Disclosure statement

The authors declare no conflict of interest.

References

1 Barnes DE, Yaffe K. The projected effect of risk factor reduction on Alzheimer's disease prevalence. *Lancet Neurol* 2011; **10**: 819–828.
2 Biessels GJ, Staekenborg S, Brunner E, Brayne C, Scheltens P. Risk of dementia in diabetes mellitus: a systematic review. *Lancet Neurol* 2006; **5**: 64–74.
3 Querfurth HW, LaFerla FM. Alzheimer's disease. *N Engl J Med* 2010; **362**: 329–344.
4 Schrijvers EM, Witteman JC, Sijbrands EJ, Hofman A, Koudstaal PJ, Breteler MM. Insulin metabolism and the risk of Alzheimer disease: the Rotterdam Study. *Neurology* 2010; **75**: 1982–1987.
5 Whitmer RA, Karter AJ, Yaffe K, Quesenberry CP Jr, Selby JV. Hypoglycemic episodes and risk of dementia in older patients with type 2 diabetes mellitus. *JAMA* 2009; **301**: 1565–1572.
6 Rizzo MR, Marfella R, Barbieri M *et al.* Relationships between daily acute glucose fluctuations and cognitive performance among aged type 2 diabetic patients. *Diabetes Care* 2010; **33**: 2169–2174.
7 Wrighten SA, Piroli GG, Grillo CA, Reagan LP. A look inside the diabetic brain: contributors to diabetes-induced brain aging. *Biochim Biophys Acta* 2009; **1792**: 444–453.
8 Luchsinger JA. Diabetes, related conditions, and dementia. *J Neurol Sci* 2010; **299**: 35–38.
9 McClean PL, Parthsarathy V, Faivre E, Holscher C. The diabetes drug liraglutide prevents degenerative processes in a mouse model of Alzheimer's disease. *J Neurosci Nurs* 2011; **31**: 6587–6594.
10 Une K, Takei YA, Tomita N *et al.* Adiponectin in plasma and cerebrospinal fluid in MCI and Alzheimer's disease. *Eur J Neurol* 2011; **18**: 1006–1009.
11 Sims-Robinson C, Kim B, Rosko A, Feldman EL. How does diabetes accelerate Alzheimer disease pathology? *Nat Rev Neurol* 2010; **6**: 551–559.
12 Peila R, Rodriguez BL, Launer LJ. Type 2 diabetes, APOE gene, and the risk for dementia and related pathologies: the Honolulu-Asia Aging Study. *Diabetes* 2002; **51**: 1256–1262.
13 Beeri MS, Silverman JM, Davis KL *et al.* Type 2 diabetes is negatively associated with Alzheimer's disease neuropathology. *J Gerontol A Biol Sci Med Sci* 2005; **60**: 471–475.
14 Matsuzaki T, Sasaki K, Tanizaki Y *et al.* Insulin resistance is associated with the pathology of Alzheimer disease: the Hisayama study. *Neurology* 2010; **75**: 764–770.
15 Arvanitakis Z, Schneider JA, Wilson RS *et al.* Diabetes is related to cerebral infarction but not to AD pathology in older persons. *Neurology* 2006; **67**: 1960–1965.
16 Ahtiluoto S, Polvikoski T, Peltonen M *et al.* Diabetes, Alzheimer disease, and vascular dementia: a population-based neuropathologic study. *Neurology* 2010; **75**: 1195–1202.
17 Ott A, Stolk RP, van Harskamp F, Pols HA, Hofman A, Breteler MM. Diabetes mellitus and the risk of dementia: the Rotterdam Study. *Neurology* 1999; **53**: 1937–1942.
18 Beeri MS, Schmeidler J, Silverman JM *et al.* Insulin in combination with other diabetes medication is associated with less Alzheimer neuropathology. *Neurology* 2008; **71**: 750–757.
19 Longstreth WT Jr, Bernick C, Manolio TA, Bryan N, Jungreis CA, Price TR. Lacunar infarcts defined by magnetic

resonance imaging of 3660 elderly people: the Cardiovascular Health Study. *Arch Neurol* 1998; **55**: 1217–1225.
20 Vermeer SE, Den Heijer T, Koudstaal PJ, Oudkerk M, Hofman A, Breteler MM. Incidence and risk factors of silent brain infarcts in the population-based Rotterdam Scan Study. *Stroke* 2003; **34**: 392–396.
21 Araki Y, Nomura M, Tanaka H *et al.* MRI of the brain in diabetes mellitus. *Neuroradiology* 1994; **36**: 101–103.
22 den Heijer T, Vermeer SE, van Dijk EJ *et al.* Type 2 diabetes and atrophy of medial temporal lobe structures on brain MRI. *Diabetologia* 2003; **46**: 1604–1610.
23 Schmidt R, Launer LJ, Nilsson LG *et al.* Magnetic resonance imaging of the brain in diabetes: the Cardiovascular Determinants of Dementia (CASCADE) Study. *Diabetes* 2004; **53**: 687–692.
24 Minoshima S, Giordani B, Berent S, Frey KA, Foster NL, Kuhl DE. Metabolic reduction in the posterior cingulate cortex in very early Alzheimer's disease. *Ann Neurol* 1997; **42**: 85–94.
25 Mistur R, Mosconi L, Santi SD *et al.* Current Challenges for the Early Detection of Alzheimer's Disease: brain Imaging and CSF Studies. *J Clinl Neurol (Seoul, Korea)* 2009; **5**: 153–166.
26 Baker LD, Cross DJ, Minoshima S, Belongia D, Watson GS, Craft S. Insulin resistance and Alzheimer-like reductions in regional cerebral glucose metabolism for cognitively normal adults with prediabetes or early type 2 diabetes. *Arch Neurol* 2011; **68**: 51–57.
27 Furumoto S, Okamura N, Iwata R, Yanai K, Arai H, Kudo Y. Recent advances in the development of amyloid imaging agents. *Curr Top Med Chem* 2007; 7: 1773–1789.
28 Kudo Y, Okamura N, Furumoto S *et al.* 2-(2-[2-Dimethylaminothiazol-5-yl]ethenyl)-6- (2-[fluoro]ethoxy) benzoxazole: a novel PET agent for in vivo detection of dense amyloid plaques in Alzheimer's disease patients. *J Nucl Med* 2007; **48**: 553–561.
29 Okamura N, Fodero-Tavoletti MT, Kudo Y *et al.* Advances in molecular imaging for the diagnosis of dementia. *Expert Opin Med Diagn* 2009; **3**: 705–716.
30 Arai H, Okamura N, Furukawa K, Kudo Y. Geriatric medicine, Japanese Alzheimer's disease neuroimaging initiative and biomarker development. *Tohoku J Exp Med* 2010; **221**: 87–95.
31 Furukawa K, Okamura N, Tashiro M *et al.* Amyloid PET in mild cognitive impairment and Alzheimer's disease with BF-227: comparison to FDG-PET. *J Neurol* 2010; **257**: 721–727.
32 McKhann G, Drachman D, Folstein M, Katzman R, Price D, Stadlan EM. Clinical diagnosis of Alzheimer's disease: report of the NINCDS-ADRDA Work Group under the auspices of Department of Health and Human Services Task Force on Alzheimer's Disease. *Neurology* 1984; **34**: 939–944.
33 Matsui T, Higuchi M, Okamura N, Arai H, Sasaki H. A practical method to predict rate of cognitive decline in mild to moderate Alzheimer's disease. *Neurology* 1999; **53**: 2208–2209.
34 Fazekas F, Kleinert R, Offenbacher H *et al.* Pathologic correlates of incidental MRI white matter signal hyperintensities. *Neurology* 1993; **43**: 1683–1689.
35 Zhao WQ, De Felice FG, Fernandez S *et al.* Amyloid beta oligomers induce impairment of neuronal insulin receptors. *FASEB J* 2008; **22**: 246–260.